Omega-3 polyunsaturated fatty acids impinge on CD4+ T cell motility and adipose tissue distribution via direct and lipid mediator-dependent effects

Cucchi, Danilo; Camacho-muñoz, Dolores; Certo, Michelangelo; Niven, Jennifer; Smith, Joanne; Nicolaou, Anna; Mauro, Claudio

DOI:
10.1093/cvr/cvz208

ESC European Society of Cardiology
Cardiovascular Research
doi:10.1093/cvr/cvz208

Omega-3 polyunsaturated fatty acids impinge on CD4$^+$ T cell motility and adipose tissue distribution via direct and lipid mediator-dependent effects

Danilo Cucchi [1†], Dolores Camacho-Muñoz[2†], Michelangelo Certo [3], Jennifer Niven[3], Joanne Smith [1], Anna Nicolaou [2,4*‡], and Claudio Mauro [1,3,5,6*‡]

[1]William Harvey Research Institute, Barts and The London School of Medicine and Dentistry, Queen Mary University of London, Charterhouse Square, London EC1M 6BQ, UK; [2]Laboratory for Lipidomics and Lipid Biology, Division of Pharmacy and Optometry, Faculty of Biology, Medicine and Health, School of Health Sciences, The University of Manchester, Manchester Academic Health Science Centre, Oxford Road, Manchester M13 9PT, UK; [3]Institute of Inflammation and Ageing, College of Medical and Dental Sciences, University of Birmingham, Mindelsohn Way, Birmingham B15 2WB, UK; [4]Lydia Becker Institute of Immunology and Inflammation, Faculty of Biology, Medicine and Health, The University of Manchester, Manchester Academic Health Science Centre, Oxford Road, Manchester M13 9PT, UK; [5]Institute of Cardiovascular Sciences, College of Medical and Dental Sciences, University of Birmingham, Mindelsohn Way, Birmingham B15 2WB, UK; and [6]Institute of Metabolism and Systems Research, College of Medical and Dental Sciences, University of Birmingham, Mindelsohn Way, Birmingham B15 2WB, UK

Received 25 January 2019; revised 16 July 2019; editorial decision 26 July 2019; accepted 1 August 2019

Time for primary review: 17 days

Aims Adaptive immunity contributes to the pathogenesis of cardiovascular metabolic disorders (CVMD). The omega-3 polyunsaturated fatty acids (n-3PUFA) are beneficial for cardiovascular health, with potential to improve the dysregulated adaptive immune responses associated with metabolic imbalance. We aimed to explore the mechanisms through which n-3PUFA may alter T cell motility and tissue distribution to promote a less inflammatory environment and improve lymphocyte function in CVMD.

Methods and results Using mass spectrometry lipidomics, cellular, biochemical, and *in vivo* and *ex vivo* analyses, we investigated how eicosapentaenoic acid (EPA) and docosahexaenoic acid (DHA), the main n-3PUFA, modify the trafficking patterns of activated CD4$^+$ T cells. In mice subjected to allogeneic immunization, a 3-week n-3PUFA-enriched diet reduced the number of effector memory CD4$^+$ T cells found in adipose tissue, and changed the profiles of eicosanoids, octadecanoids, docosanoids, endocannabinoids, 2-monoacylglycerols, N-acyl ethanolamines, and ceramides, in plasma, lymphoid organs, and fat tissues. These bioactive lipids exhibited differing chemotactic properties when tested in chemotaxis assays with activated CD4$^+$ T cells *in vitro*. Furthermore, CD4$^+$ T cells treated with EPA and DHA showed a significant reduction in chemokinesis, as assessed by trans-endothelial migration assays, and, when implanted in recipient mice, demonstrated less efficient migration to the inflamed peritoneum. Finally, EPA and DHA treatments reduced the number of polarized CD4$^+$ T cells *in vitro*, altered the phospholipid composition of membrane microdomains and decreased the activity of small Rho GTPases, Rhoα, and Rac1 instrumental in cytoskeletal dynamics.

Conclusions Our findings suggest that EPA and DHA affect the motility of CD4$^+$ T cells and modify their ability to reach target tissues by interfering with the cytoskeletal rearrangements required for cell migration. This can explain, at least in part, the anti-inflammatory effects of n-3PUFA supporting their potential use in interventions aiming to address adipocyte low-grade inflammation associated with cardiovascular metabolic disease.

Keywords n-3PUFA • CD4$^+$ T cell • Adipose tissue • Cardiovascular metabolic disease • Mass spectrometry lipidomics

* Corresponding authors. Tel: +44 (0) 161 2752374; E-mail: anna.nicolaou@manchester.ac.uk (A.N.); Tel: +44 (0)121 371 7892; E-mail: c.mauro@bham.ac.uk (C.M.)

† The first two authors contributed equally to the study and considered as first authors.

‡ The last two authors contributed equally to the study and considered as senior authors.

1. Introduction

Chronic low-grade inflammation is a key feature of cardiovascular metabolic disorders (CVMD), a group of diseases where T cell-mediated adaptive immunity has been considered to play an important role.[1–3] T cells infiltrate atherosclerotic plaques and obese adipose tissue, driving disease progression through pro-inflammatory immune responses mediated by $CD4^+$ T-helper type 1 (Th1) and $CD8^+$ cytotoxic T lymphocytes preponderant over immunomodulatory (Th2) and immunosuppressive (T regulatory - Treg) immunity.[1,2] Recruitment and activation of macrophages release of pro-inflammatory cytokines while altered regulatory mechanisms further perpetuate inflammation.[1,4] As we have recently shown, fat overload leads to a biased differentiation of a pro-inflammatory effector memory-like population of $CD4^+$ T cells, both in humans and mice, contributing to the low-grade inflammation observed in obesity.[5]

The omega-3 (n-3) polyunsaturated fatty acids (PUFA) eicosapentaenoic (EPA) and docosahexaenoic (DHA) acids, found in fish oils, have been explored as means of preventing cardiovascular disease and improving cardiometabolic risk factors.[6–8] Although the efficiency of n-3PUFA is debated, recent clinical studies have shown that EPA supplementation can reduce the risk of ischemic events and increase the stability of the atherosclerotic plaque, with EPA plaque levels inversely related to their T cell content.[9–12] Furthermore, n-3PUFA suppress antigen presentation, activation, and proliferation, and lower the expression of cytokines by T cells.[13–15] While the immunomodulatory properties of n-3PUFA are appreciated, the underpinning molecular mechanisms are not fully understood. Recent findings indicate that EPA induces the differentiation of regulatory T cells through the up-regulation of peroxisome proliferator-activated receptor γ,[16] while DHA alters the composition and molecular organization of membrane microdomains, with consequent changes in the activity of signalling proteins linked to actin remodelling, overall, leading to reduced $CD4^+$ T cell activation.[17–19]

Further to altering membrane composition, n-3PUFA can dispense activities via their metabolism to bioactive lipid mediators of inflammation and immunity, many of which are key players in the cardiovascular system.[17,20,21] Membrane esterified omega-6 (n-6) PUFA, such as linoleic acid (LA) and arachidonic acid (AA), compete with n-3PUFA for the same enzymes and yield an array of pro- and anti-inflammatory eicosanoids, octadecanoids, and docosanoids, including pro-resolving mediators (e.g. resolvins, protectins, maresins).[20–22] Endocannabinoids and other N-acyl ethanolamines (NAE) are PUFA derivatives with strong involvement in the cardiovascular system, inflammation, and immunity.[21,23] n-3PUFA can also influence the production of ceramides, potent lipid mediators of cell differentiation, and apoptosis, also involved in insulin metabolism and lipotoxicity underpinning cardiovascular disease.[24–26]

Systemically and locally produced lipid mediators interact with T cells through cell surface receptors affecting activation, differentiation, proliferation, cytokine production, motility, and homing events.[21] Examples include the pro-inflammatory and immunosuppressive prostaglandin E_2 (PGE_2) that stimulates differentiation of lymphocytes influencing the development and balance of Th1, Th2, and Th17 subsets in a concentration-dependent manner,[21,27] the endocannabinoid anandamide (AEA) that inhibits T cell proliferation and was shown to be immunosuppressive,[28] and ceramide-1-phosphate (C1P) that promotes cell migration although its effect on T cell function remains to be explored.[29,30]

Modifying the trafficking patterns of activated T cells can promote a less inflammatory environment and improve cardiovascular health; therefore, in-depth understanding of the mechanisms underpinning the n-3PUFA effects on T cell-mediated immune responses is of importance. As well as elucidating the currently debated role of EPA and DHA on cardiovascular health, such detailed insight can support improved interventions and reveal the identity of lipid species with immune-modulatory activities that could instigate the design of novel therapeutics. In this study, we used mice subjected to allogeneic immunization after a diet supplemented with n-3PUFA. Altered distribution of activated $CD4^+$ T cells in fat tissues revealed the impact of n-3PUFA on the ratio of effector to central memory $CD4^+$ T cells, while mediator lipidomics revealed bioactive lipids with differing chemotactic properties, formed systemically and in the target tissues. Treating $CD4^+$ T cells with EPA and DHA *ex vivo* showed that n-3PUFA could modify membrane microdomains and regulate the signalling events involved in the cytoskeletal dynamics influencing the T cell migratory capabilities.

2. Materials and methods

2.1 Animal study

All *in vivo* experiments were conducted under the UK Home Office regulation and conformed to the guidelines from Directive 2010/63/EU of the European Parliament on the protection of animals used for scientific purposes. All animals were euthanized via exposure to rising concentration of CO_2, according to humane schedule 1 procedures. To study the effect of n-3PUFA supplementation on T cell distribution and composition, wild-type (WT) C57BL/6 female mice were randomly allocated to groups ($n = 5$ animals per group) fed either chow diet (CD) or CD supplemented with 10% salmon oil (CD + ω3) for 3 weeks (Supplementary material online, *Table S1*) [Special Diet Service (SDS)], as previously reported.[31] Immunization was performed during the third week of supplementation (Section 2.2).

2.2 T cell activation

In vitro: murine $CD4^+$ T cells were isolated with commercially available isolation kits (negative selection; EasySep, Invitrogen) according to the manufacturer's instructions from pooled lymph nodes (inguinal, mesenteric, axillary, brachial, superficial and deep cervical, lumbar, and sacral) and spleen of C57BL/6 female mice and activated with plate bound anti-CD3 (1 mg/mL, eBioscience), anti-CD28 (5 mg/mL, eBioscience), and IL-2 (10 ng/mL, Roche) for 3–4 days; they were then treated overnight with EPA or DHA (free fatty acids dissolved in ethanol) (20 μM; Cambridge Bioscience) as previously reported;[32] this was followed by a treatment with CXCL10 (300 ng/mL) for 1 h with or without methyl-β-cyclodextrin (MβCD; 5 mM; Sigma). Alternatively, on the third day of activation, T cells were treated overnight with the indicated lipid mediators (free forms dissolved in ethanol) (10 nM; Cambridge Bioscience).

In vivo: in WT C57BL/6 female mice fed CD or CD + ω3 for 3 weeks, memory $CD4^+$ T cells were generated by i.p. immunization with WT Balb/c and CD-1 male splenocytes (1.5×10^6) for 7 days. T cells were then isolated from mesenteric (draining) lymph nodes (mLNs), spleen, cardiac fat, perigonadal fat, and subcutaneous fat and used for flow cytometry.

2.3 Peritoneal recruitment

In vitro activated $CD4^+$ T cells were pre-treated with EPA or DHA (20 μM), labelled with 7-hydroxy-9H-(1,3-dichloro-9,9-dimethylacridin2-one) (DDAO) (Invitrogen) and intravenously injected in recipient syngeneic female C57BL/6 mice (5×10^6 cells/mouse) that had 3 h prior

received an intraperitoneal injection with CXCL10 (1200 ng/mouse) (n = 4–6 animals); 24 h later, peritoneal lavage and spleen were collected and analysed by FACS for presence of DDAO-labelled T cells.

2.4 Membrane and intracellular FACS staining

Spleen samples were lysed of their RBCs before staining. Dead cells were excluded from analysis by staining with fixable Aqua Dead Cell Stain (Invitrogen). Isolated lymphocytes were stained for surface markers: CD4, CD44, CD62L, LFA1, CXCR3, and CD25 (*Figure 1A–F*, n = 3–5 animals per group; *Figure 4B*, n = 4–6, *Figure 4C*, n = 3 independent experiments; Supplementary material online, *Figure S3A–C*, n = 3 independent experiments) with fluorescently conjugated primary antibodies (1:200, eBioscience/BioLegend) at 4°C for 30 min in FACS buffer [phosphate buffered saline (PBS) + 2% FCS + 0.1% sodium azide] and fixed at 4°C for 30 min with 1% PFA in FACS buffer. For intracellular staining, isolated lymphocytes were incubated in permeabilization/fixation buffer (eBioscience) at 4°C for 1 h. Samples were washed in permeabilization buffer and stained for Foxp3 (1:200, eBioscience/BioLegend) with fluorescently conjugated primary antibodies at 4°C for 30 min in permeabilization buffer. In Supplementary material online, *Figure S3D*, proliferation of CD4$^+$ T cells was assessed by dilution of CFSE (3.3 μM, Invitrogen) (n = 9 independent experiments). All samples were then assessed by flow cytometry using an LSRFortessa (BD Biosciences) and FlowJo version 10 software. Dot plots were concatenated to show the independent biological replicates used in each experiment.

2.5 Isolation of lymphocytes from fat tissue

Cardiac, perigonadal, and subcutaneous fat were harvested from mice fed CD or CD + ω3 for 3 weeks, cut in small pieces and suspended in a solution of PBS + 5% BSA containing Collagenase Type II (Sigma) and calcium chloride. Samples were incubated for 20 min at 37°C in agitation to allow tissue digestion; they were then filtered through a 70 μm cell strainer and the collected cell suspension was washed and stained for FACS analysis. Any blood contamination was removed by lysis of red cells with RBC lysis buffer. The weight of the fat tissues harvested from all animals used is shown in Supplementary material online, *Table S2*.

2.6 Chemotaxis

Chemotaxis assays were performed in 5 μm transwell inlays (Corning). *In vitro* activated lymphocytes were suspended in migration medium (RPMI 2% FCS) and seeded in the upper transwell chamber (3×10^5 cells/transwell). Chemokine CXCL10 (300 ng/mL) (PeproTech) was added to the lower chamber, or alternatively the indicated lipid mediators at a concentration of 10 nM or other as indicated. Migrated T cells were counted with a haemocytometer at 2, 4, and 6 h after seeding, and then the percent of migrated cells was calculated (n = 7 animals in *Figure 3A and B*; n = 3 animals in *Figure 4D*). In some assays, microvascular endothelial cells (isolated from the lungs of C57BL/6 mice) were seeded (3×10^4 cells/well) on 3 μm transwell inlays.[33] On the following day, T cells (3×10^5 cells/well) suspended in migration medium were added to the top chamber of the transwell and incubated at 37°C with 5% CO_2 to allow migration through the endothelial monolayers. Migrated T cells were counted with a haemocytometer at 6 and 24 h after seeding, then the percent of migrated cells was calculated (*Figure 4A*, n = 3 independent experiments).

2.7 Cytotoxicity assay

Cytotoxicity was assessed by the MTT assay performed using the CellTiter 96 AQueous One Solution Cell Proliferation colorimetric assay (Promega), according to the manufacturer's instructions. Briefly: *in vitro* activated T cells (5×10^4 cells) were treated overnight with increasing fatty acid concentrations (1–100 μM); they were then seeded into each well of a 96-well plate and CellTiter 96 AQueous One Solution reagent was added (20 μL per well). After 1 h incubation, absorbance (490 nm) was measured in a microplate reader (n = 3 independent experiments; Supplementary material online, *Figure S3F*).

2.8 Western blot

Protein lysates were prepared from CD4$^+$ T lymphocytes isolated from pooled lymph nodes and activated as described above. Samples were lysed in Nonidet P-40 lysis buffer (50 mM HEPES pH 8.0, 350 mM NaCl, 1% Nonidet P-40, 1 mM EDTA, 1 mM Na_3VO_4, 1 mM NaF, 20 mM glycerol-2-phosphate, 1 mM PMSF, 1 mM DTT, 10 mg/mL aprotinin, 10 mg/mL leupeptin, and a protease inhibitor mixture; Roche). Equivalent amounts of protein as determined by standard Bradford assay (Bio-Rad) were separated by SDS/PAGE and transferred to a Nylon membrane (GE Healthcare). Membranes were blocked for 1 h at room temperature in 5% Milk/TBS-T, incubated overnight at 4°C with primary antibodies (1:1000), and subsequently with horseradish peroxidase-conjugated secondary antibody (Amersham Bioscience) (1:5000). Antibodies against Rhoα and Rac1 were purchased from Cytoskeleton, Inc. p-PAK1/2, p-MLC2, and b-actin were purchased from Cell Signalling. Pull-down of the active form of Rhoα and Rac1 were performed, respectively, with Rhotekin-RBD protein GST beads and PAK-GST protein beads according to the manufacturer's instruction.

2.9 Immunofluorescence

CD4$^+$ T cells isolated from lymph nodes and spleen of C57BL/6 female mice were activated *in vitro* for 3 days; on the third day of activation, cells were treated overnight with EPA, DHA, or oleic acid (20 μM) (n = 3 independent experiments). The day after, cells were treated with CXCL10 300 ng/mL for 1 h and, where indicated, with MβCD (5 mM; Sigma) (n = 3 independent experiments); then cells were suspended in PBS and allowed to attach for 1 h in incubator at 37°C onto coverslips pre-treated with Cell-tack (Corning). Cells were then washed, fixed in 3.7% PFA for 20 min, permeabilized with PBS containing 0.2% Triton X-100, blocked with PBS containing 1% BSA and 0.02% Triton X-100 for 30 min and incubated with 6.6 μM Phalloidin (F-actin staining, Thermo Fisher Scientific) and 0.3 μM Dnasel (G-actin staining, Thermo Fisher Scientific) for 30 min. Anti-Rhoα (Cytoskeleton, Inc.) mouse antibody was incubated for 2 h (1:100) and revealed with anti-mouse Alexa fluor 569 for 45 min. Nuclei were stained with DAPI (300 nM; Thermo Fisher Scientific). Finally, coverslips were mounted onto slides using a DAKO mounting medium. Images were acquired using a confocal microscopy and analysed using ZEN software; in Supplementary material online, *Figure S5*, images were acquired using a fluorescence microscope (Leica AF60000) and LAS X Software.

2.10 Mediator lipidomics

Extraction and analysis of prostanoids and hydroxy fatty acids was performed as described previously.[34,35] Briefly, plasma (100–200 μL) or solid tissue (20–60 mg) samples (n = 6 animals per group) were homogenized in ice-cold methanol (15% v/v), spiked with a mixture of deuterated internal standards (40 ng each of 12-HETE-*d8*, 8,9-DHET-d11,

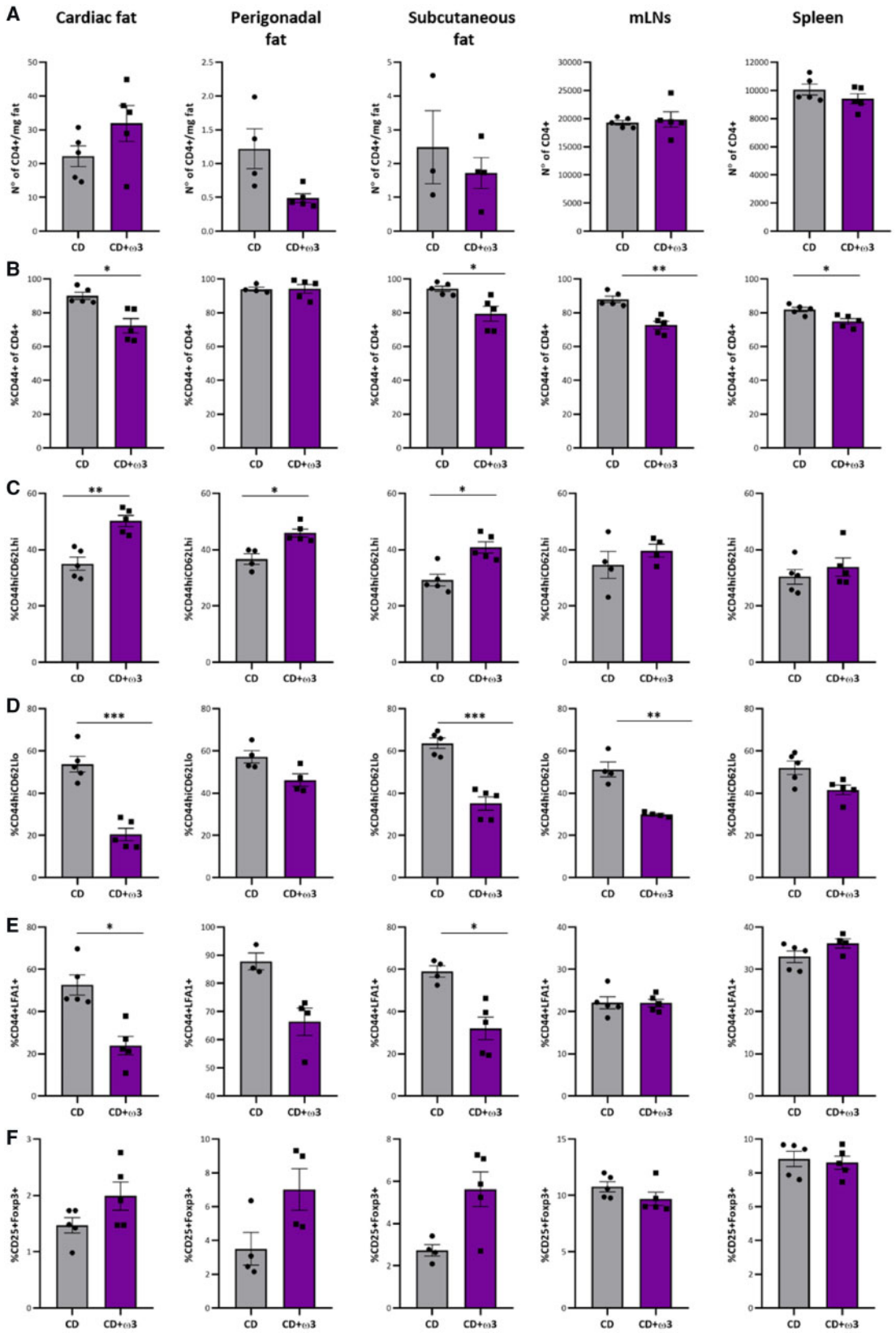

Figure 1 n-3PUFA supplementation alters the distribution of T cell subsets in fat tissue and lymphoid organs. (*A–F*) Cell surface staining of CD4 (*A*), CD44 (*B*), CD62L (*C* and *D*), LFA1 (*E*), CD25, and Foxp3 (*F*) in *in vivo* primed $CD4^+$ T cells isolated from the indicated tissues of female C57BL/6 WT mice fed a chow (CD) or chow with 10% salmon oil (CD + ω3) diet for 3 weeks. In (A), the absolute number of $CD4^+$ T cells in cardiac, perigonadal, and subcutaneous fat has been normalized to the amount of tissue (mg) harvested. Multiple *t*-tests followed by Holm Sidak *post-hoc* correction ($n = 3–5$ animals per group). Values denote mean ± SEM. $^*P < 0.05$; $^{**}P < 0.01$; and $^{***}P < 0.001$.

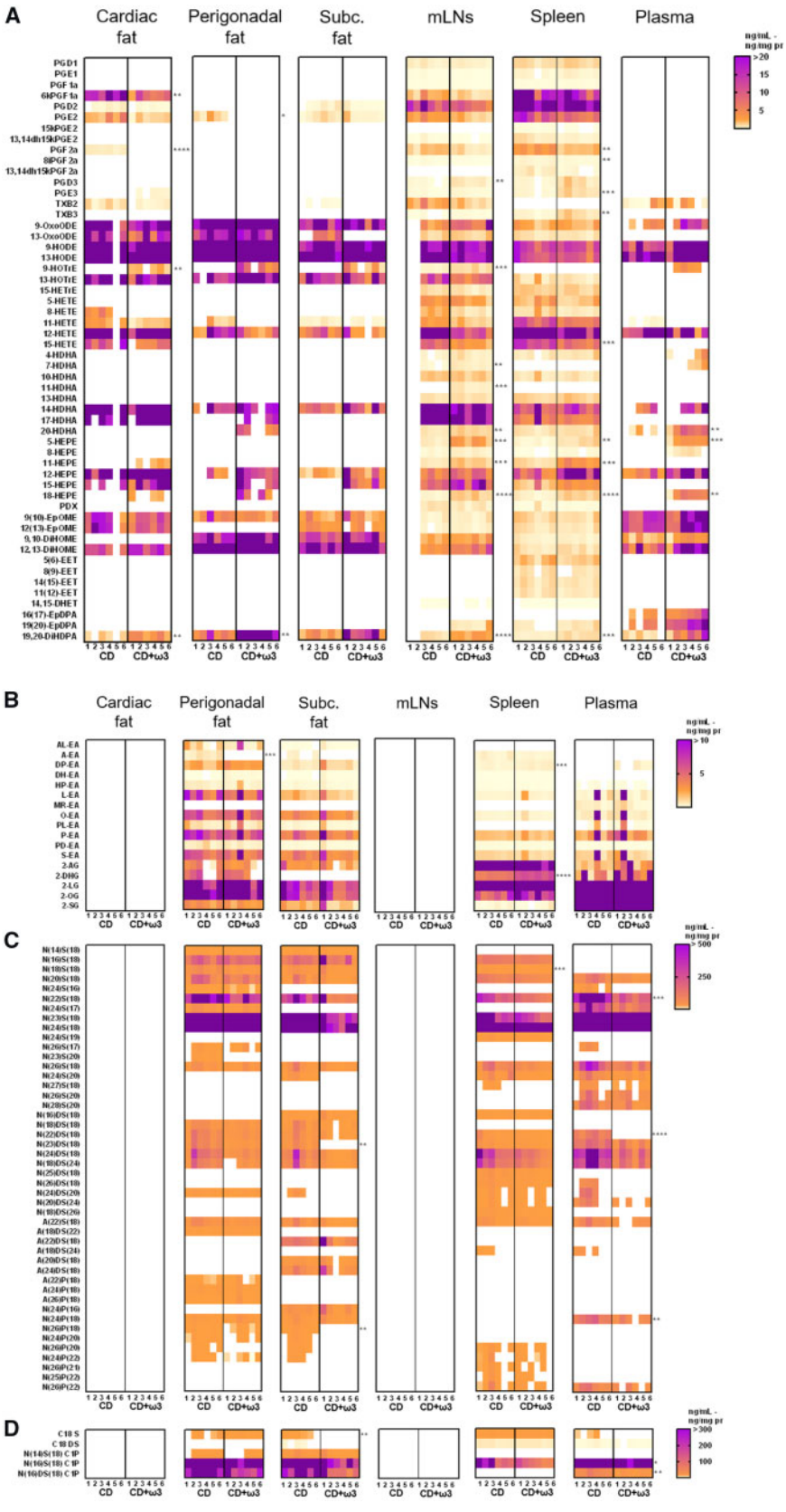

Figure 2 Effect of n-3PUFA supplementation on eicosanoids, docosanoids, and octadecanoids (*A*), endocannabinoids and N-acyl ethanolamines (*B*) and ceramides (*C*), sphingoid bases and phosphorylated ceramides (*D*) found in fat tissue, lymphoid organs, and plasma. Tissue was obtained from female C57BL/6 WT mice fed a chow (CD) or chow with 10% salmon oil (CD + ω3) diet. Data are expressed as ng/mg protein in solid tissues and ng/mL in plasma. *$P < 0.05$, **$P < 0.01$, ***$P < 0.001$, and ****$P < 0.0001$ based on multiple *t*-tests followed by Holm Sidak *post-hoc* correction ($n = 6$ animals per group).

8,9-EET-*d11*, and PGB_2-*d4*) and incubated in the dark. Solid phase extraction (SPE) (C18 cartridges; Phenomenex, Macclesfield, UK) was used to clean-up the supernatants, which were then acidified and added to the pre-conditioned SPE cartridges. Lipids were eluted with methyl formate and analysed by ultrahigh performance chromatography (UPLC; Acquity, Waters, USA) coupled to a triple quadrupole mass spectrometer with an electrospray ionization source (Xevo TQS, Waters) (UPLC/ESI-MS/MS) in the negative ionization mode on a C18 column (Acquity UPLC BEH C18; 50 × 2.1 mm, 1.7 µm; Waters, UK). Instrument and data analysis were carried out by TargetLynx software (Waters, UK). Data reported were normalized with the use of internal standards and quantified using internal calibration curves constructed with commercially available standards.

Extraction and analysis of endocannabinoids, NAE, 2-monoacylglycerols (MG), ceramides, phosphorylated ceramides, phosphorylated bases, and free sphingoid bases were performed as described.[34,36] Briefly, plasma (100–200 µL) or solid tissue (20–60 mg) samples were homogenized in ice-cold chloroform/methanol (2:1, v/v), spiked with a mixture of internal standards [20 ng of AEA-*d8* and 40 ng of 2-AG-*d8*, 20 ng of CERN(18)S(18)-*d3*, 20 ng of CERN(16)DS(18)-*d9* and CERA(16)S(18)-*d9* and 50 pmol of Cer/Sph Mixture I; Cayman Chemicals, Ann Arbour, MI, USA; Avanti Polar Lipids, USA], and incubated in the dark. Analytes were recovered in the organic layer and analysed by UPLC/ESI-MS/MS using a C18 column (Acquity UPLC BEH C18; 50 × 2.1 mm, 1.7 µm; Waters, UK) for endocannabinoids and NAE, and a C8 column (Acquity UPLC BEH C8; 100 × 2.1 mm; 1.7 µm; Waters, UK) for ceramides; all in the positive ionization mode. In the case of solid tissues the organic layer was cleaned up by SPE (Strata SI-1-Silica; Phenomenex, Macclesfield, UK) before their analysis by UPLC/ESI-MS/MS. Instrument and data analysis were carried out by TargetLynx software (Waters, UK). Data reported were normalized using internal standards; endocannabinoids, 2-MG, and NAE were quantified using internal calibration curves constructed with commercially available standards; relative quantification of ceramides was performed using internal standards.

Protein content was performed on the protein pellets retained during the lipid extractions using protein assay kit (Bio-Rad, Hemel Hempstead, UK), as described.[34]

2.11 Isolation and lipid analysis of detergent-resistant membrane microdomains

The insolubility of membrane microdomains in non-ionic detergents, such as Brij-58, at 4°C is the most common method used to isolate detergent-resistant membranes (DRM); low density DRM are a crude representation of 'lipid raft microdomains'. Here, DRM were isolated from murine T cells (*Figure 6A*, $n = 4$ independent experiments; *Figure 6B and C*, $n = 5$ independent experiments) as described before.[37] Briefly, T cells were lysed with a lysis buffer (100 mM NaCl, 2 mM EDTA, 4.1 mM AEBSF, 0.2 mM Na_3VO_4, 50 µM NaF, 25 mM HEPES, 3.2 µM aprotinin, 88 µM leupeptin, 160 µM bestain, 60 µM pepstain A, and 56 µM E-64, pH 6.9) containing 1% Brij-58. Cell lysates were passed through a 27G needle once and incubated on ice in the dark. Cell lysates were mixed with 330 µL of 85% sucrose prepared in lysis buffer. Then, 1 mL of 35% sucrose and 300 µL of 5% sucrose were subsequently overlaid. Samples were ultracentrifuged at 200 000 *g* (Beckman Coulter Optima Max-E ultracentrifuge, TLS 55 rotor) overnight at 4°C. Then, 10 aliquots of 200 µL were collected from the top to the bottom sequentially, to generate 10 fractions (Fr. 1–5% sucrose; Fr. 2–9.2% sucrose; Fr. 3–13.3% sucrose, Fr. 4–17.5% sucrose; Fr. 5–21.7% sucrose; Fr. 6–25.8% sucrose; Fr. 7–30.0% sucrose; Fr. 8–34.2% sucrose; Fr. 9–38.3% sucrose; Fr. 10–42.5% sucrose).

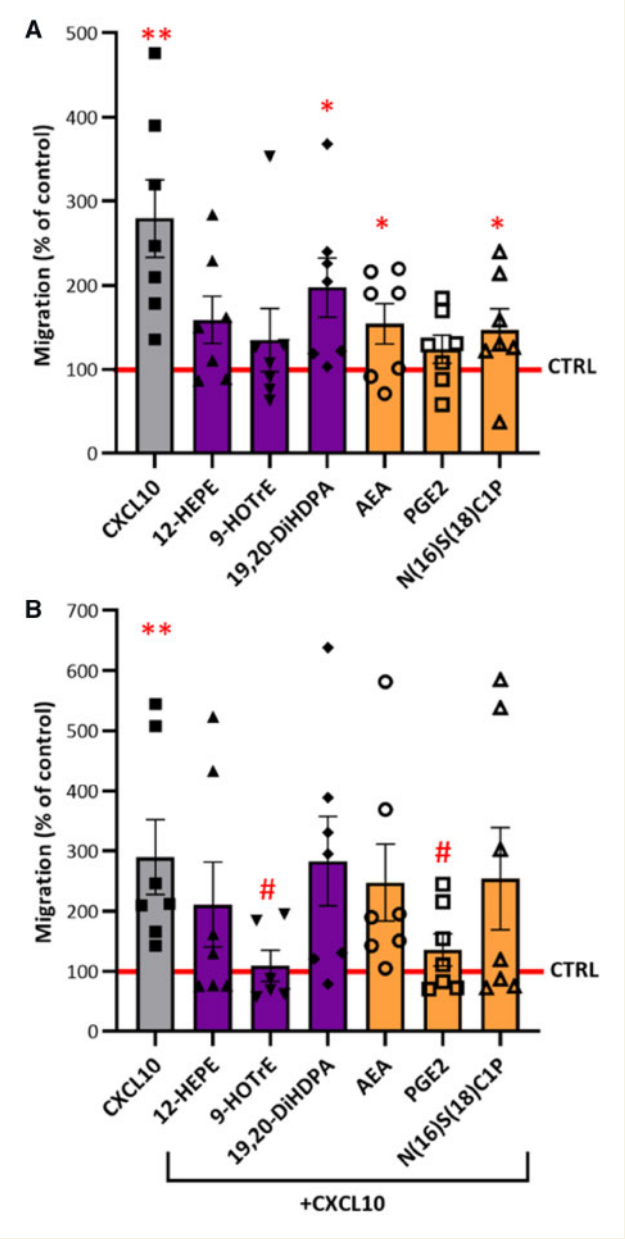

Figure 3 Lipid mediators affect $CD4^+$ T cell migration, *in vitro*. Chemotaxis assay of *in vitro* activated $CD4^+$ T cells isolated from pooled lymph nodes and spleens of female C57BL/6 WT mice in response to the cytokine CXCL10 (300 ng/mL), the eicosanoids PGE_2 and 12-HEPE, the octadecanoid 9-HOTrE, the docosanoid 19, 20-DiHDPA, the endocannabinoid AEA, and C1P N(16)S(18)C1P (10 nM), the combination of the cytokine and lipid treatment, or media only (indicated by the red line; CTRL). In (*A*), lipid mediators are tested for their ability to affect $CD4^+$ T cells migratory capabilities; conversely, in (*B*) their capacity to counteract or synergize with CXCL10 is measured. The number of migrated cells is reported as a percentage normalized to media only control. Two-tailed Student's *t*-test ($n = 7$ independent experiments). The values denote mean ± SEM. $^*P < 0.05$; $^{**}P < 0.01$ vs. CTRL (red line); and $^{\#}P < 0.05$ vs. CXCL10 (*B*).

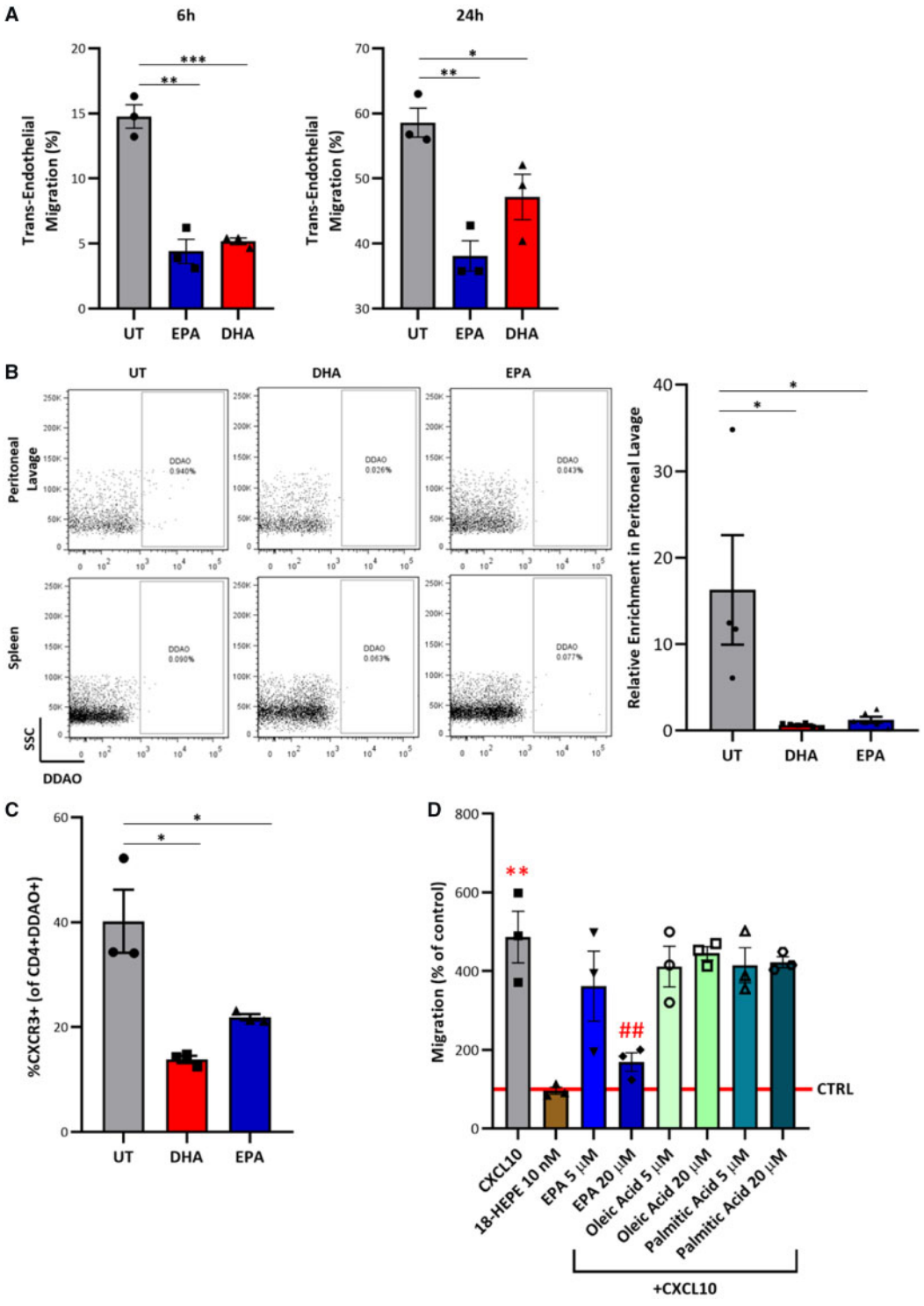

Figure 4 EPA and DHA reduce the migratory capacity of CD4^{+} T cells, both *in vitro* and *in vivo*. (*A*) Trans-endothelial migration (6 h and 24 h time points) of *in vitro* activated CD4^{+} T cells in the presence of EPA (20 µM) or DHA (20 µM). (*B*) Relative enrichment of i.v.-injected activated CD4^{+} T cells pre-treated with EPA (20 µM) or DHA (20 µM) and subsequently labelled with 7-hydroxy-9H-(1,3-dichloro-9,9-dimethylacridin2-one) (DDAO) cell fluorescent dye in the peritoneal lavage of syngeneic recipient C57BL/6 mice i.p.-injected with CXCL10 (1200 ng/mouse). (*C*) Cell surface staining of the CXCL10 receptor CXCR3 in CD4^{+}DDAO^{+} T cells isolated from the peritoneal lavage of mice in (*B*). UT denotes untreated control cells. (*D*) Chemotaxis assay of *in vitro* activated CD4^{+} T cells isolated from pooled lymph nodes and spleens of female C57BL/6 WT mice in response to the chemokine CXCL10 (300 ng/mL) or the eicosanoid 18-HEPE (10 nM); also EPA (5 and 20 µM), Oleic acid (5 and 20 µM) and Palmitic acid (5 and 20 µM) in combination with CXCL10, or media only (indicated by the red line; CTRL). Two-tailed Student's *t*-test [(*A*) $n = 3$ independent experiments; (*B*) $n = 4$–6 animals per group; (*C*) $n = 3$ animals per group; (*D*) $n = 3$ independent experiments]. The values denote mean ± SEM. $^{*}P < 0.05$; $^{**}P < 0.01$; $^{***}P < 0.001$; and $^{\#\#}P < 0.01$ vs. CXCL10 (*D*).

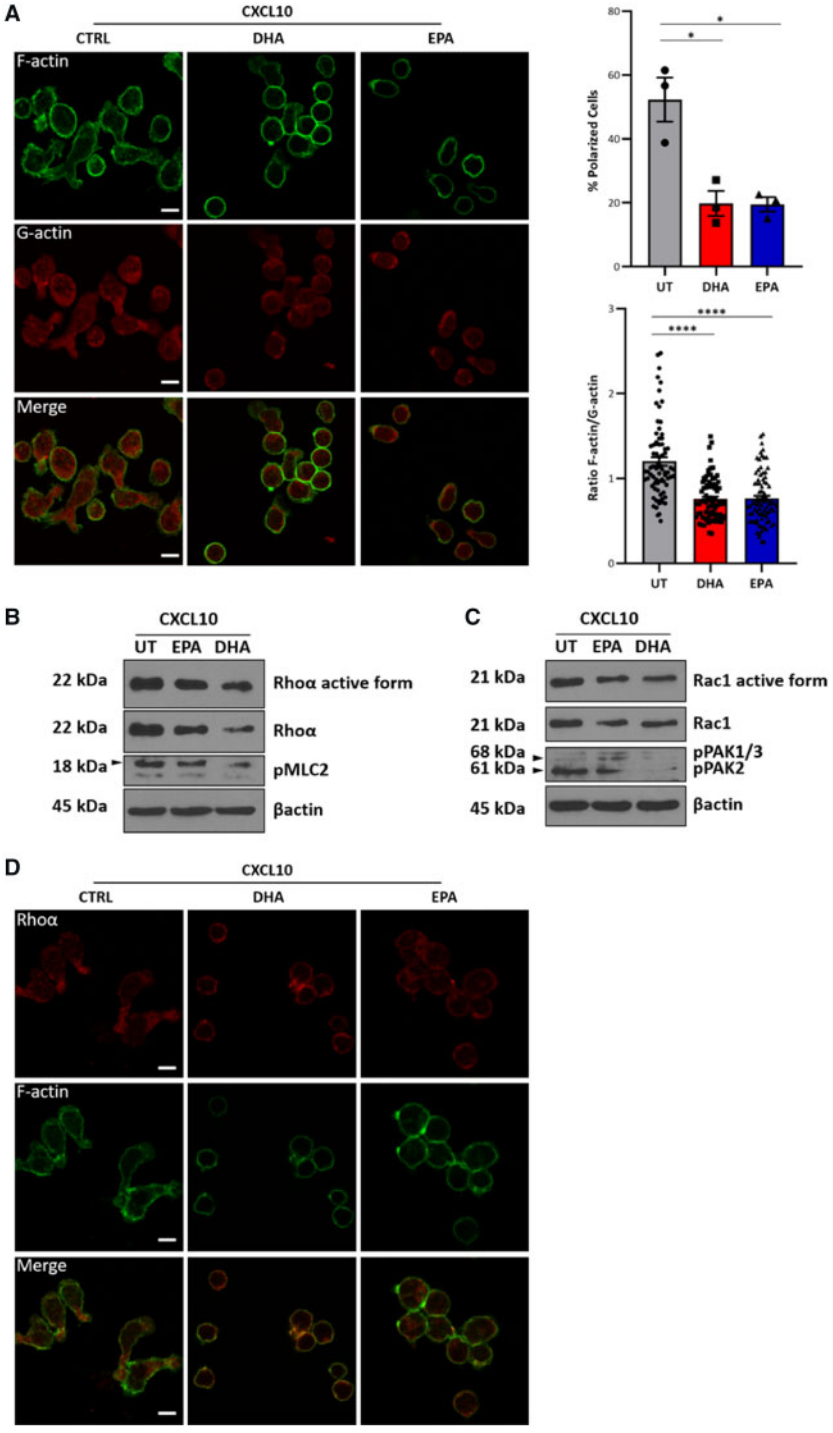

Figure 5 EPA and DHA alter the polarization of $CD4^+$ T cells and down-regulate the expression of small Rho GTPases. (*A*) Double immunofluorescence staining for F-actin (green) and G-actin (red) in *in vitro* activated $CD4^+$ T cells, overnight treated with EPA (20 μM) and DHA (20 μM) and stimulated with the cytokine CXCL10 (300 ng/mL) for 1 h prior to fixation. Quantification of the % of polarized cells is provided upon counting polarized cells (cells showing one or more pseudopods) in at least 10 images per condition. The ratio F-actin/G-actin is calculated using the intensity of the staining as provided by the software used for the acquisition and analysis of the images (ZEN), each dot represents a single cell analysed (an average of 30 cells were analysed in each experiment). Images were acquired using a confocal microscope. Scale bar = 10 μm. (*B* and *C*) Western blot analysis of Rhoα (total and activated), phospho-MLC2, Rac1 (total and activated), phospho-PAK1/2, and β-actin in *in vitro* activated $CD4^+$ T cells overnight treated with EPA (20 μM) or DHA (20 μM) and stimulated with CXCL10 (300 ng/mL) for 1 h prior to lysis; UT denotes untreated control cells. (*D*) Double immunofluorescence staining for F-actin (green) and Rhoα (red) in *in vitro* activated $CD4^+$ T cells, overnight treated with EPA (20 μM) and DHA (20 μM) and stimulated with CXCL10 (300 ng/mL) for 1 h prior to fixation. Scale bar = 10 μm. Two-tailed Student's *t*-test ($n = 3$ independent experiments). The values denote mean ± SEM. $^*P < 0.05$ and $^{****}P < 0.0001$.

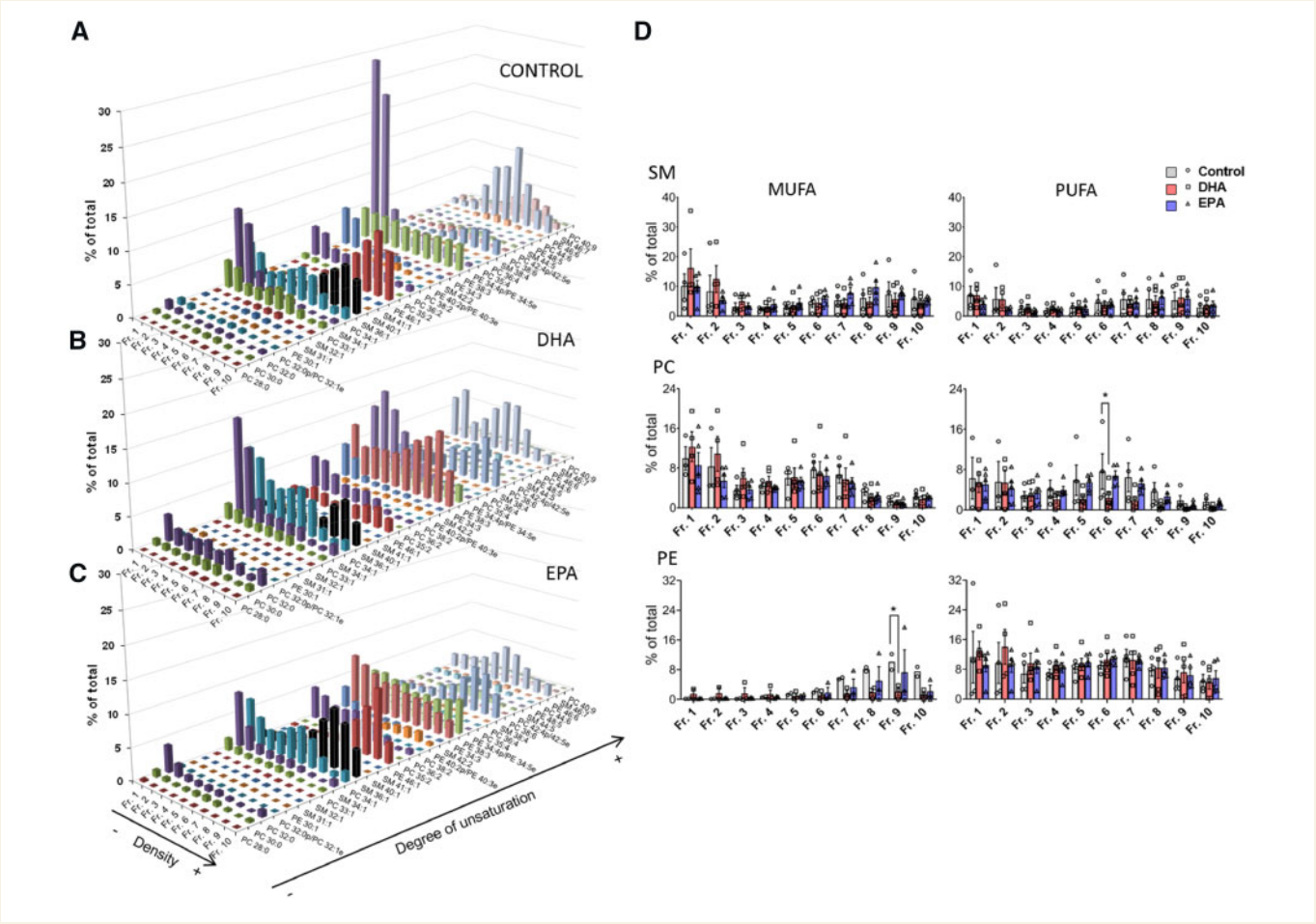

Figure 6 Distribution of sphingomyelin (SM), phosphatidylcholine (PC), and phosphatidylethanolamine (PE) species in untreated (*A*), DHA-treated (*B*), or EPA-treated (*C*) CD4$^+$ T cell membrane microdomains and the distribution of monounsaturated (MUFA) and polyunsaturated fatty acids (PUFA) (*D*). Cells were lysed with detergent (Brij-58; 1%) and membranes fractionated by ultracentrifugation using a sucrose gradient, with density increasing from fraction 1 (Fr. 1–5% sucrose) to fraction 10 (Fr. 10–42.5% sucrose). The relative abundance of lipid species in each fraction was estimated by supercritical fluid chromatography coupled to time of flight mass spectrometry. The composition of membrane microdomains separated by each sucrose fraction is shown as increased degree of unsaturation of the relevant lipid species. Data are expressed as % of total. *$P < 0.05$ based on one-way ANOVA followed by Tukey *post-hoc* test ($n = 4$–5 independent experiments).

Extraction and analysis of membrane lipids were performed as described before.[38] Briefly: sucrose gradient fractions (200 µL) were mixed with ice-cold chloroform/methanol (2:1, v/v), spiked with a mixture of internal standards [200 µg each of palmitic acid-*d31*, 15:0 cholesteryl-*d7* ester, 16:0-*d31*-18:1 phosphatidylcholine, 16:0-*d31*-18:1 phosphatidylethanolamine, 17:0-17:1-17:0-*d5* triacylglycerol; 26:0-*d4* lysophosphatidylcholine, 16:0-*d31* sphingomyelin (SM), 18:1-*d5* diacylglycerol and 18:1-*d7* lysophosphatidylethanolamine, and 400 µg cholesterol-*d7*] (Avanti Polar Lipids) and incubated on ice in the dark. The organic layer containing the lipids was recovered by centrifugation after the addition of water, evaporated to dryness and reconstituted in chloroform/2-propanol (1:1, v/v). Lipid analysis was carried out by ultra-high-performance supercritical fluid chromatography (UHPSFC; Acquity UPC^2, Waters) coupled to a quadrupole-time-of-flight mass spectrometer (Synapt G2 High Definition Q-TOF, Waters, Milford, MA, USA) (UHPSFC/ESI-QTOF-MS^E), in the positive and negative ionization mode, using an Acquity UPC^2 Torus 2-PIC column (Waters). Instrument and data analysis were carried out by TargetLynx software (Waters, UK). Data processing was carried out using Progenesis QI (Waters), which aided TIC-based chromatogram alignment and peak picking. Lipid identification was performed and confirmed through fragmentation patterns, using the LIPID MAPS database and in-house information. Relative quantification was estimated using deuterated internal standards.

2.12 Statistical analysis

Data are expressed as mean ± standard error of the mean (SEM), using $n = 3$–6 animals per group (*Figures 1, 2, and 4*) and $n = 3$–7 independent experiments per group (*Figures 3–7*), unless otherwise stated in the methods section. Data distribution was assessed for normality using the Shapiro–Wilk and Kolmogorov–Smirnov normality tests. For the cell and animal studies, the data were parametric. The lipidomics data were mainly parametric although the distribution of some lipid species in some of the tissues examined was not parametric. We therefore analysed the data with parametric and non-parametric tests and performed sensitivity tests in the raw and log transformed data; in all cases we came

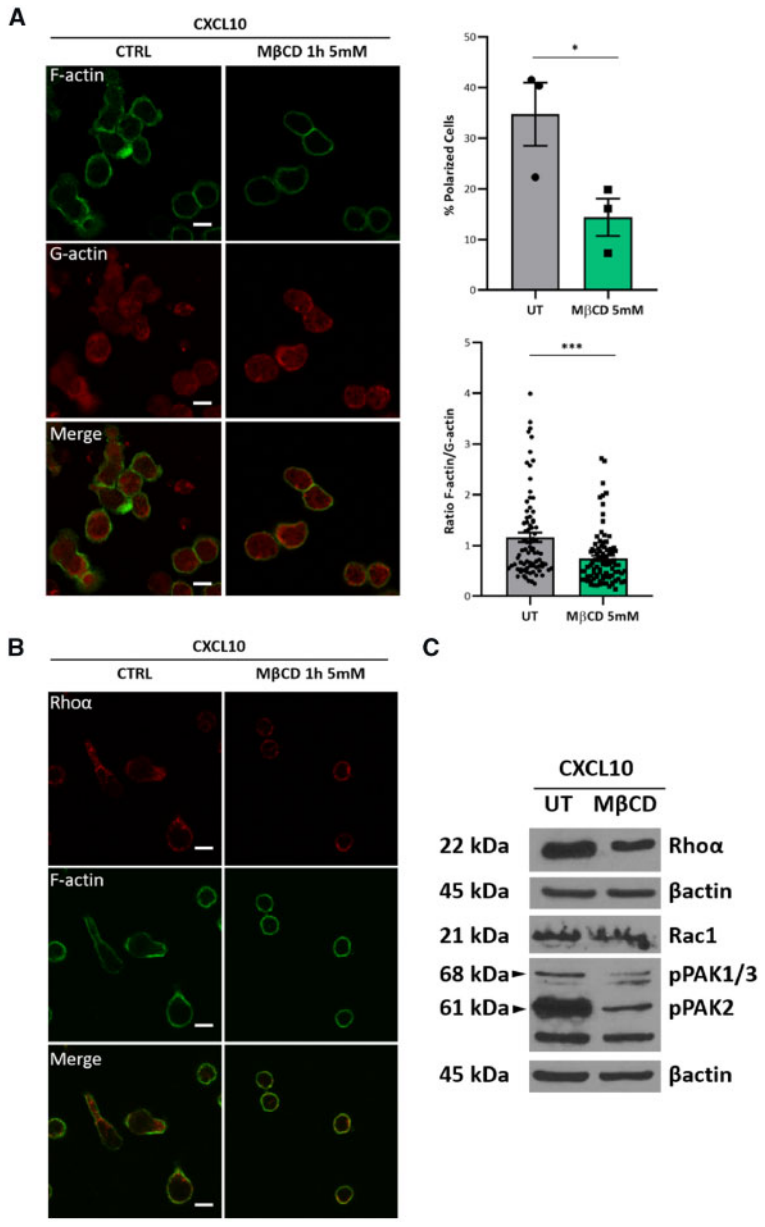

Figure 7 Disruption of lipid rafts recapitulates the effect of EPA and DHA on the cytoskeletal dynamics of $CD4^+$ T cells. (*A*) Double immunofluorescence staining for F-actin (green) and G-actin (red) in *in vitro* activated $CD4^+$ T cells treated with methyl-β-cyclodextrin (MβCD) (5 mM) for 1 h in the presence of the cytokine CXCL10 (300 ng/mL). Quantification of the % of polarized cells is provided upon counting polarized cells (cells showing one or more pseudopods) in at least 10 images per condition. The ratio F-actin/G-actin is calculated using the intensity of the staining as provided by the software used for the acquisition and analysis of the images (ZEN), each dot represents a single cell analysed (an average of 30 cells were analysed in each experiment). Images were acquired using a confocal microscope. Scale bar = 10 µm. (*B*) Double immunofluorescence staining for F-actin (green) and Rhoα (red) in *in vitro* activated $CD4^+$ T cells, treated with MβCD (5 mM) in the presence of CXCL10 (300 ng/mL) for 1 h prior to fixation. Scale bar = 10 µm. (*C*) Western blot analysis of Rhoα, Rac1, phospho-PAK1/2, and β-actin in *in vitro* activated $CD4^+$ T cells treated with MβCD (5 mM) for 1 h in the presence of CXCL10 (300 ng/mL) and untreated control (UT). Two-tailed Student's *t*-test ($n = 3$ independent experiments). The values denote mean ± SEM. $^*P < 0.05$ and $^{***}P < 0.001$.

up with similar results, therefore the initial analysis using parametric tests was applied. The tests used were two-tailed Student's *t*-tests and multiple *t*-tests with Holm Sidak *post-hoc* test for multiple comparisons or one-way ANOVA with Tukey *post-hoc* test. All analyses were performed using GraphPad Prism version 7.00. In all cases, a *P*-value of <0.05 was considered to be significant.

3. Results

3.1 Tissue distribution of $CD4^+$ T cells post n-3PUFA supplementation

The effect of n-3PUFA supplementation on the distribution of the main $CD4^+$ T cell subsets in adipose tissues and lymphoid organs was

examined. No major changes in body parameters, including weight, were observed after 3 weeks of CD + ω3 diet compared to CD, which was in line with our previous data.[6] Lymphoid organs (spleen and mLNs) and adipose tissue from different areas of the body, namely the heart (cardiac fat), lower peritoneum (perigonadal fat), and skin (subcutaneous fat) were harvested 7 days after immunization and the number and subtypes of CD4$^+$ T cells were assessed by FACS. We found that, in the n-3PUFA supplemented animals (CD + ω3 group), the overall number of CD4$^+$ T cells (as normalized to fat tissue weight; Supplementary material online, *Table S2*), was not significantly different as compared to untreated controls (CD group); similarly, no difference was observed in the number of CD4$^+$ T cells found in the lymphoid organs (*Figures 1A* and Supplementary material online, Figure *S1A*).

Dietary supplementation with n-3PUFA also led to a reduction in the relative abundance of activated memory CD44$^+$ T cells (assessed as % of total CD4$^+$ T cells), both in fat (with the only exception of perigonadal fat) and lymphoid tissues (*Figure 1B* and Supplementary material online, Figure *S1B*). Importantly, the n-3PUFA diet altered the balance between central and effector memory CD4$^+$ T cell populations in the fat tissues examined, leading to a statistically significant reduction in the CD44^{hi}CD62L^{lo} (cardiac fat $P < 0.001$, subcutaneous fat $P < 0.001$, mLNs $P < 0.01$) and CD44$^+$LFA1$^+$ (cardiac fat $P < 0.05$, subcutaneous fat $P < 0.05$) effector memory CD4$^+$ T cell population, while it increased the CD44^{hi}CD62L^{hi} central memory CD4$^+$ T cell subset (cardiac fat $P < 0.01$, perigonadal fat $P < 0.05$, subcutaneous fat $P < 0.05$) (*Figure 1C–E* and Supplementary material online, Figure *S1C and D*, respectively). Furthermore, analysis of the regulatory CD25$^+$Foxp3$^+$ (Treg) CD4$^+$ T cells, showed a trend towards an increase in the Treg population found in the fat tissues of animals fed the n-3PUFA-supplemented diet, as compared to animals fed standard CD (*Figure 1F* and Supplementary material online, Figure *S1E*).

3.2 Tissue profiling of lipid mediators post n-3PUFA supplementation

As CD4$^+$ T cell function may be affected by chemotactic lipid mediators, we employed lipidomics performed by UPLC/ESI-MS/MS[34–36,39] to analyse various eicosanoids, docosanoids, octadecanoids, endocannabinoids, NAE, 2-MG, ceramides, and sphingoid bases, in plasma, spleen, lymphoid, and adipose tissues of the animals fed CD and CD + ω3 diets (*Figure 2*).

Although mLNs and spleen had the largest number and diversity of cyclooxygenase-derived (COX) prostanoids and lipoxygenase (LOX-) and cytochrome P450 (CYP-) hydroxy- and epoxy-fatty acids detected (all members of the eicosanoid, octadecanoid, and docosanoid classes), cardiac, perigonadal, and subcutaneous fat and plasma appeared to produce the most abundant species at higher concentrations (*Figure 2A*). The n-3PUFA diet reduced levels of AA-derived prostanoids and increased EPA- and dihomo-γ-linolenic acid (DGLA)-derived species in all tissues examined. Specifically: statistical significant decrease of $PGF_{2\alpha}$ in cardiac fat ($P < 0.0001$) and spleen ($P < 0.01$), PGE_2 in perigonadal fat ($P < 0.05$), and prostacyclin (measured as 6-keto $PGF_{1\alpha}$) in cardiac fat ($P < 0.01$) were observed, while levels of 8-*iso*-$PGF_{2\alpha}$ ($P < 0.01$), PGE_3 ($P < 0.001$), and TXB_3 ($P < 0.01$) in spleen and PGD_3 ($P < 0.01$) in mLNs were significantly increased. Furthermore, the n-3PUFA supplementation reduced most AA-, α-linolenic acid- and DGLA-derived mediators formed via the LOX and CYP pathways, with concomitant increases in DHA-, EPA- and LA-derived species. The following mediators were significantly increased: 9-HOTrE in cardiac fat ($P < 0.01$) and mLNs ($P < 0.001$); 7-HDHA ($P < 0.01$) in mLNs; 11-HDHA ($P < 0.001$) in mLNs; 5-HEPE in mLNs ($P < 0.001$), spleen ($P < 0.01$), and plasma ($P < 0.001$); 20-HDHA in mLNs ($P < 0.01$) and plasma ($P < 0.01$); 11-HEPE in mLNs ($P < 0.001$) and spleen ($P < 0.001$); 18-HEPE in mLNs ($P < 0.0001$), spleen ($P < 0.0001$), and plasma ($P < 0.01$); and 19,20-DiHDPA in mLNs ($P < 0.0001$) and spleen ($P < 0.001$). 15-HETE was significantly decreased in spleen ($P < 0.001$).

Due to limited sample availability, endocannabinoids, NAE, 2-MG, and ceramides were only analysed in perigonadal and subcutaneous fat, spleen, and plasma (*Figure 2B–D*). Although plasma showed the highest concentrations of 2-MG species, 2-AG was found mostly in spleen. Interestingly, the fish oil diet significantly reduced production of AEA ($P < 0.001$) in perigonadal fat, while the n-3PUFA-derived species DPEA ($P < 0.001$) and 2-DHG ($P < 0.0001$) were significantly increased in spleen (*Figure 2B*).

CER[NS] and CER[NDS] were the main ceramide classes detected in all tissues examined; CER[NS] species containing fatty acyl chains of C14–C18 were found mainly in fat tissues, whereas CER[NS] with longer acyl chains, i.e. C26–C28, were mostly present in plasma. The highest number of CER[NDS] ceramides was found in spleen. The less abundant CER[NP] ceramides were present in adipose tissue and spleen, whereas CER[ADS] and CER[AP] were found only in fat tissues (*Figure 2C and D*). Overall, the n-3PUFA diet, appeared to reduce the number of ceramides, with most significant changes observed in plasma and subcutaneous fat. In detail: CERN(22)S(18) ($P < 0.001$), N(22)DS(18) ($P < 0.0001$), N(24)P(18) ($P < 0.01$), N(16)S(18)C1P ($P < 0.05$), and N(16)DS(18)C1P ($P < 0.01$) were reduced in plasma; N(23)DS(18) ($P < 0.01$), N(26)P(18) ($P < 0.01$), and C18S ($P < 0.01$) were lower in subcutaneous fat; and N(18)S(18) ($P < 0.001$) was reduced in spleen. Additionally, a significant reduction was observed in ceramides with C22 fatty acyl chain ($P < 0.01$) in plasma and a significant increase in ceramides with C16 fatty acyl chain ($P < 0.01$) in subcutaneous fat, in the n-3PUFA fed group compared to mice fed on CD (Supplementary material online, *Figure S2*).

3.3 n-3PUFA and related mediators directly affect T cell motility and trafficking

The observed altered tissue distribution of CD4$^+$ T cells can be caused by EPA and/or DHA-induced changes in the production of chemotactic lipid mediators, both systemically and in the target fat tissues. We therefore examined the activity of selected lipid species, namely: the eicosanoids PGE_2, 12-HEPE and 18-HEPE, the octadecanoid 9-HOTrE, the docosanoid 19, 20-DiHDPA, the endocannabinoid AEA, and the C1P N(16)S(18)C1P, and assessed their ability to affect the motility of CD4$^+$ T cells in *ex vivo* assays. The bioactive lipids selected represent the classes of mediators that were found mostly affected by the fish oil diet; their activity was assessed at a single concentration (10 nM) that corresponds to the lower level these mediators were found in the tissues analysed (*Figures 2, 3, and 4D*).

Lipid mediators can act as chemoattractants but can also affect the migratory response of T cells to chemokines;[30,40–43] we therefore assessed both potential modalities of action. When tested for their chemotactic activity, 19,20-DiHDPA, AEA, and N(16)S(18)C1P appeared to significantly increase the migratory response of activated CD4$^+$ T cells (*Figures 3A and 4D*). Conversely, when tested for their ability to interfere with the migratory response to the control chemokine CXCL10, CD4$^+$ T cells pre-treated with 9-HOTrE and PGE_2 showed reduced ability to migrate, compared to CXCL10 alone (*Figure 3B*).

EPA and DHA were also assessed for their direct impact on the ability of CD4$^+$ T cells to migrate across an endothelial monolayer. Activated

$CD4^+$ T cells were treated with EPA and DHA (20 μM; 16 h) and allowed to interact with interferon-γ-primed endothelial monolayer. Both EPA and DHA reduced the trans-endothelial migration of $CD4^+$ T cells, at 6 h and 24 h after seeding, compared to vehicle control (*Figure 4A*). This effect was weaker at 24 h showing that the n-3PUFA-induced inhibition is reversible. Furthermore, both EPA and DHA pre-treated cells showed impaired traffic to the inflamed peritoneum, *in vivo* (*Figure 4B*). Moreover, the n-3PUFA treatment reduced the proportion of $CXCR3^+$ (CXCL10 receptor) in the population of fluorescently labelled $CD4^+$ T cells that had reached the peritoneum (*Figure 4C*), while no difference was observed in the $CD44^{high}CCR7^{low}$ or $CD44^{high}CD62L^{low}$ $CD4^+$ T cells (Supplementary material online, *Figure S3A*). The inhibitory effect of n-3PUFA to the chemotactic response to CXCL10 was specific as no effects were observed with the monounsaturated fatty acid oleic acid or the saturated fatty acid palmitic acid (*Figure 4D*).

Finally, we assessed whether EPA and DHA could induce the differentiation of $CD4^+$ T cells to a central memory subset which would explain the reduced migration through an activated endothelium as well as the reduced trafficking to the CXCL10-enriched peritoneum. However, we did not observe any significant effects (Supplementary material online, *Figure S3B and C*). Furthermore, treatment with EPA and/or DHA (20 μM, 16 h) (Supplementary material online, *Figure S3D and E*), or with a 1–100 μM concentration range of EPA, or oleic acid or palmitic acid (Supplementary material online, *Figure S3F*) did not alter proliferation or survival of $CD4^+$ T cells as compared to vehicle treatment.

3.4 EPA and DHA affect cell polarization and cytoskeleton dynamics

The impact of EPA and DHA on cytoskeletal dynamics, a process underpinning all migratory events, was explored using $CD4^+$ T cells treated with EPA, DHA (20 μM) *in vitro*. Actin remodelling was followed by staining of filamentous actin (F-actin) and globular actin (G-actin), the two main forms actin is present in cells (*Figure 5A*, left). The n-3PUFA treatment caused a reduction in the number of polarized $CD4^+$ T cells, i.e. cells with a leading edge (pseudopod), in the presence of the pro-migratory stimulus CXCL10 (*Figure 5A*, top right). Although a similar trend was observed in the absence of CXCL10, the number of spontaneously polarized cells was low, and the results did not reach statistical significance (Supplementary material online, *Figure S4A*). Furthermore, the F-actin/G-actin ratio—a measure of how dynamic the cytoskeleton is—was also reduced by both EPA and DHA, consistent with the observed reduced polarization (*Figure 5A*, bottom right). The monounsaturated fatty acid oleic acid did not show the same effect as EPA or DHA on cell morphology (Supplementary material online, *Figure S5*), confirming the specificity of n-3PUFA.

Further mechanistic insight was sought by analysing the expression of the small Rho GTPase, Rhoα and Rac1, two key orchestrators of cell polarization and migration.[44,45] Treatment of activated $CD4^+$ T cells with EPA and/or DHA in the presence or absence of CXCL10, caused a reduction of Rhoα and Rac1 total protein levels as well as of the active, GTP-bound form, which is responsible of the regulation of the cytoskeletal dynamics (*Figure 5B and C* and Supplementary material online, Figure *S4B*).

To assess the potential functional consequences of the observed n-3PUFA-induced Rhoα and Rac1 down-regulation, we analysed the phosphorylation levels of the downstream target of Rhoα and Rac1, MLC2 and PAK1/2, respectively,[46–48] and found that they were both decreased (*Figure 5B and C*). Finally, staining Rhoα and F-actin in EPA- and DHA-treated $CD4^+$ T cells, with or without CXCL10, showed distinct patterns of localization of Rhoα: while most untreated control cells were polarized with Rhoα mainly found at the pseudopods (*Figure 5D*), the majority of EPA- and DHA-treated cells had a round shape with Rhoα showing an even distribution along the cell membrane or in the cytoplasm (*Figure 5D*).

3.5 n-3PUFA affect the distribution of glycerophospholipids and SMs in $CD4^+$ T cell membrane microdomains

EPA and DHA can modify the lipid composition of the plasma membrane and this can affect the formation and structure of the membrane microdomains important for delivering signals that modify the cytoskeletal dynamics.[49–52] The impact of n-3PUFA on the lipid composition of $CD4^+$ T cell membrane microdomains was explored through profiling of membrane lipids by UHPSFC/ESI-QTOF-MS^E. For this, we analysed the relative abundance and distribution of glycerophospholipids, sphingolipids, and acylglycerides in DRM fractions prepared from $CD4^+$ T cells treated *ex vivo* with EPA, DHA (20 μM), or vehicle (control) using a sucrose gradient (*Figure 6* and Supplementary material online, Figures *S6–S8*). The low density DRM separated in Fr. 1–3 roughly represent 'lipid rafts'.[37]

In control untreated T cells, the predominant SM species were SM 34:1, SM 36:1, SM 38:4, SM 42:2, and SM 46:7 (*Figure 6A*). Profiling individual SM species across the 10 gradient fractions showed an enrichment of SM 34:1 and SM 42:2 in the DRM (Fr. 1–3) and SM 36:1, SM 38:4, and SM 46:7 in the high density detergent soluble membrane (DSM) fractions (Fr. 8–10) (Supplementary material online, *Figure S6A*). The most abundant glycerophosphatidylcholine (PC) species were PC 33:1, PC 34:1, and PC 36:2. While saturated, monounsaturated and polyunsaturated PC species were enriched in the DRM (Fr. 1–3) and intermediate density (Fr. 4–7) fractions, PC species containing more than two double bonds were found enriched in the intermediate density fractions (Fr. 4–7) (*Figure 6A and D* and Supplementary material online, Figures *S6B and S7*). Glycerophosphatidylethanolamines (PE) were less abundant than SM and PS. The main PE species identified were PE 30:1, PE 34:4p/34:5e, PE 38:3, PE 46:6, and PE 46:1; although these were found distributed across all density fractions, monounsaturated PE species were found enriched in DSM fractions (Fr. 8–10) (*Figure 6A and D* and Supplementary material online, Figure *S6C*). Finally, triacylglycerides were found mostly in either the DRM (Fr. 1–3) or DSM (Fr. 8–10) fractions (Supplementary material online, *Figure S6E*), whereas diacylglycerides were found mostly accumulated in the intermediate density fractions (Fr. 4–7) (Supplementary material online, *Figure S6F*).

Treatment with DHA altered the lipid composition of the membrane microdomains, across the sucrose gradient fractions (*Figure 6A–D* and Supplementary material online, Figures *S6A–F, S7, and S8*). Although the distribution of total phospholipids and acylglycerides did not change, the relative abundance of lipid species was altered. In detail: DHA caused an enrichment of monounsaturated SM, PC, and PE species in the DRM fractions and reduced polyunsaturated PC species in the intermediate density fractions (Fr. 4–7) ($P < 0.05$) and monounsaturated PE species in the DSM fractions (Fr. 8–10) ($P < 0.05$), all compared to untreated controls (*Figure 6D* and Supplementary material online, Figure *S8*). Conversely, EPA was less effective that DHA and had no effect on the re-distribution of SM and PC species, although it appeared to shift monounsaturated PE species to the DRM (*Figure 6A* and Supplementary material online, *Figure S6C*). The observed changes suggest that DHA is more

efficient than EPA in modifying DRM membrane structures, with potential implications for the fluidity of the cellular membrane and impact upon related signalling pathways.

3.6 Lipid microdomain disruption exerts the same effect as EPA and DHA treatment

The impact of EPA and DHA on membrane microdomains may also disrupt the signalling pathways to Rho GTPase proteins downstream of chemokine signalling.[52] To test this hypothesis, CXCL10-stimulated CD4$^+$ T cells were treated *in vitro* with the cyclodextrin MβCD, a high molecular weight cyclic oligosaccharide able to deplete cholesterol from biological membranes, thus impeding lipid microdomain formation.[53] This resulted in a reduction in cell polarization and F-actin/G-actin ratio, similar to that observed following T cell treatment with EPA and DHA (*Figure 7A*). The expression of the small Rho GTPase, Rhoα, and Rac1 was also reduced (*Figure 7C*) while the cellular distribution of Rhoα was altered in a way similar to the EPA and DHA treatments, showing an even distribution around the plasma membrane as compared to the pseudopod accumulation in the CXCL10-treated cells (*Figure 7B*).

4. Discussion

The importance of adaptive immunity in the establishment of a chronic, low-grade inflammation in CVMD is now becoming clear and new interventions are needed to combat this unwanted inflammatory response and re-establish physiological tissue homeostasis. The anti-inflammatory protective effects of n-3PUFA extend to the cardiovascular and immune systems, and here we examined their impact on the properties and tissue distribution of CD4$^+$ T cells, crucial orchestrators of inflammatory responses in cardiometabolic disease.

The n-3PUFA supplementation modified the balance among the T cell populations reducing the pro-inflammatory T cells in most of the fat tissues examined; this was accompanied by a concomitant increase in the central memory CD44^{hi}CD62L^{hi} CD4$^+$ T cells (*Figure 1*). Our findings support the anti-inflammatory profile of n-3PUFA suggesting that their activities are mediated, at least in part, through changes in T cell properties including motility. Although not assessed here, n-3PUFA supplementation is considered beneficial in other organs including the liver where it has been shown to confer protection against damage in the setting of steatosis and high-fat diet by reducing ceramide production and regulating sphingolipid biosynthesis.[54,55]

N-3PUFA can modify the network of bioactive lipid mediators, both locally and systemically, altering the prevalence of chemotactic lipid species with consequence for the migratory capacity of T cells.[21] Profiling the mediator lipidome in the target lymphoid and fat tissues, and plasma, showed reduction of AA-derived mediators, together with increased production of EPA- and DHA-derived species, and reduction of ceramides (*Figure 2*). While AA mediators are considered pro-inflammatory, their EPA and DHA counterparts appear to be either less potent or present anti-inflammatory protective profiles, and reduced levels of ceramides have been linked to improvement in cardiovascular disease.[20,21,26]

Changes in the composition of the tissue lipid milieu may have affected the distribution pattern of locally detected CD4$^+$ T cells, therefore selected bioactive lipid species were assessed for their potency as chemoattractants as well as for their ability to interfere with the effect of CXCL10, a potent inflammatory chemokine. In the absence of any other migratory stimulus, 19,20-DiHDPA, AEA and N(16)S(18)C1P increased the migration of CD4$^+$ T cells *in vitro* (*Figure 3A*). The endocannabinoid AEA and C1P N(16)S(18)C1P were found reduced by the n-3PUFA treatment in perigonadal and subcutaneous fat, and this may have led to the decrease in CD44$^+$ T cells found in fat tissues (*Figure 1*). 19,20-DiHDPA, a product of DHA, was increased post-supplementation in all tissues examined, and its ability to act as chemoattractant may have also contributed to the CD4$^+$ T cells subtype profiles observed in lymphoid and fat tissues. 18-HEPE, a product of EPA and precursor of pro-resolving mediators was also increased post-supplementation.[56] However, unlike 19,20-DiHDPA, AEA and N(16)S(18)C1P, 18-HEPE did not have any effect on the migratory response of activated CD4$^+$ T cells. Although other studies have shown the activity of EPA- and DHA-derived pro-resolving lipids (e.g. RvE and RvD), these were not identified in the tissues analysed, suggesting that, if formed, their levels were below the level of detection of the assays used in our experimental settings.[56,57]

Our findings (*Figure 1*) are the result of multiple changes in the network of lipid mediators, all occurring as a result of the n-3PUFA diet, and the exact contribution and properties of individual species should be further explored. When assessed in the presence of CXCL10, the octadecanoid 9-HOTrE and eicosanoid PGE_2 were able to counteract the potent effect of this chemokine (*Figure 3B*). While 9-HOTrE was found increased post n-3PUFA, the levels of PGE_2 were reduced (*Figure 2A*), showing the differential contribution of various lipid mediators in the anti-inflammatory effect of n-3PUFA diets. It is therefore evident that the metabolism of n-3PUFA and subsequent perturbation of bioactive lipids have diverse effects on the migratory ability of T cells, but the overall balance is towards an anti-inflammatory protective effect suggesting that dietary supplementation may regulate the function of T cells.

Further to their metabolism to bioactive mediators, EPA and DHA may also be directly involved in the regulation of T cell migration. As shown (*Figure 4*), both fatty acids can down-regulate the migratory capability of activated CD4$^+$ T cells, *ex vivo* and, more importantly, *in vivo*, in a peritoneal recruitment assay, suggesting that some of their anti-inflammatory effects may be attributed to inhibition of immune cell migration. Interestingly, at least *in vitro*, EPA and DHA do not interfere with the differentiation of CD4$^+$ T cell subsets, or with their proliferation and survival. Therefore, the different T cell subsets found in adipose and lymphoid tissues of n-3PUFA fed mice could be due to the effect of fatty acids on trafficking rather than differentiation.

EPA and DHA could also act at cellular level altering the ability of T cells to respond to migratory stimuli. Analysis of the polarization of activated and CXCL10-stimulated CD4$^+$ T cells showed that treatment with EPA or DHA reduced formation of pseudopods and decrease the ratio between F-actin and G-actin, a measurement of cellular dynamicity.[45] Moreover, this change happened in concomitance with the down-regulation of Rhoα and Rac1, two small Rho GTPases involved in cell migration (*Figure 5*). These findings show that EPA and DHA can interfere with the molecular machinery necessary for migration to occur, and although the exact signals triggered are not yet known, our results demonstrate that n-3PUFA have a direct impact on cytoskeletal rearrangements.

The observation that EPA and DHA down-regulate the expression rather than activity of Rhoα and Rac1 (*Figure 5B* and *C*) suggest that they trigger signals able to interfere with Rhoα and Rac1 transcriptional or post-translational regulation; elucidation of these molecular signals and their control mechanisms requires further investigation. However, the consequent decrease in phosphorylation of two downstream targets,

respectively, pMLC2 and pPAK1/2, indicates that the down-regulation of Rhoα and Rac1 is functional. Furthermore, treatment with EPA or DHA changed the cellular localization of Rhoα, from the pseudopods produced upon stimulation with CXCL10, to a cytoplasmic localization. These events suggest a broader interference with membrane-related events.

To explore this further, we assessed the impact of n-3PUFA on cellular membrane composition with emphasis on the DRM microdomains, important for receptor clustering and cell signalling relevant to cell motility.[49–52] EPA and DHA treatment of $CD4^+$ T cells *ex vivo*, showed a re-distribution of phospholipid species with DHA being more efficient than EPA in increasing the relative abundance of monounsaturated SM, PC, and PE species in DRM fractions, whereas EPA only shifted monounsaturated PE species to DRMs (*Figure 6*). This observation agrees with biophysical studies suggesting that not all n-3PUFA are equivalent in altering membrane organization.[58] DRM crudely represent the 'lipid raft' microdomains that appear necessary for the correct assembly of the molecular machinery required for cell migration. However, our data shows that DHA and EPA had similar effects on the T cell motility parameters studied, therefore we can conclude that the changes in T cell 'lipid raft' composition were not sufficient to differentially alter the underlying mechanisms responsible for the physiological effects we have observed.

Overall, our results demonstrate that n-3PUFA exert their anti-inflammatory properties by acting in multiple ways: at a systemic level they modify the network of lipid mediators in fat and lymphoid tissues, thus causing the redistribution of the different $CD4^+$ T cell subsets in favour of an anti-inflammatory phenotype (dampening the pro-inflammatory immune response); at a cellular level, they can affect the cytoskeletal rearrangements required for the migration of activated $CD4^+$ T cells. Whether n-3PUFA influence the T cell response via alteration of the processes of antigen presentation remains to be further investigated. Recent findings suggest that n-3PUFA have a strong influence on the properties of B lymphocytes, macrophage subsets, and dendritic cells;[59–61] exploring the impact of systemic and cellular changes in these cells would greatly improve our understanding of the immunomodulatory activities and potential benefit of n-3PUFA supplementation. Nevertheless, the findings of this study add to the current debate of whether EPA and DHA can improve cardiovascular outcomes, and offer support to the use of n-3PUFA in addressing the low-grade inflammatory reactions accompanying cardiometabolic disease, while their molecular mechanism of action offers targets for the development of novel therapeutics and/or interventions.

Supplementary material

Supplementary material is available at *Cardiovascular Research* online.

Authors' contributions

Conceptualization: A.N. and C.M.; Methodology: D.C., D.C.-M., M.C., J.S., A.N., and C.M.; Investigation: D.C., D.C.-M., M.C., J.N., and J.S.; Analysis: D.C., D.C.-M., M.C., J.S., A.N., and C.M.; Writing—Original Draft: D.C., D.C.-M., A.N., and C.M.; Writing—Review and Editing: all authors; Visualization: D.C., D.C.-M., M.C., A.N., and C.M.; Supervision: A.N. and C.M.; Project Administration: A.N. and C.M.; Funding Acquisition: A.N. and C.M.

Acknowledgements

The authors wish to thank RS Chapkin (Texas A&M University) for laboratory protocols, Douglas Steinke for advise on statistical analysis, Marta Koszyczarek (University of Manchester) for training, and Neil O'Hara (University of Manchester) and Josephine Volker (University of Birmingham) for excellent technical support. We would like to thank NonLinear Dynamics/Waters for their support of this work.

Conflict of interest: none declared.

Funding

This work was performed with funds from the British Heart Foundation (Project Grant PG/15/105/31906) to A.N. and C.M. D.C. was supported in part by a Fellowship from the Institute Pasteur Foundation Cenci-Bolognetti. C.M. was supported by a British Heart Foundation Intermediate Basic Science Research Fellowship (FS/12/38/29640) and a start-up grant from the University of Birmingham.

References

1. Rocha VZ, Libby P. Obesity, inflammation, and atherosclerosis. *Nat Rev Cardiol* 2009;**6**:399–409.
2. Baker RG, Hayden MS, Ghosh S. NF-kappaB, inflammation, and metabolic disease. *Cell Metab* 2011;**13**:11–22.
3. Mauro C, Marelli-Berg FM. T cell immunity and cardiovascular metabolic disorders: does metabolism fuel inflammation? *Front Immunol* 2012;**3**:173.
4. Lahoute C, Herbin O, Mallat Z, Tedgui A. Adaptive immunity in atherosclerosis: mechanisms and future therapeutic targets. *Nat Rev Cardiol* 2011;**8**:348–358.
5. Mauro C, Smith J, Cucchi D, Coe D, Fu H, Bonacina F, Baragetti A, Cermenati G, Caruso D, Mitro N, Catapano AL, Ammirati E, Longhi MP, Okkenhaug K, Norata GD, Marelli-Berg FM. Obesity-induced metabolic stress leads to biased effector memory CD4(+) T cell differentiation via PI3K p110delta-Akt-mediated signals. *Cell Metab* 2017;**25**:593–609.
6. Innes JK, Calder PC. The differential effects of eicosapentaenoic acid and docosahexaenoic acid on cardiometabolic risk factors: a systematic review. *Int J Mol Sci* 2018;**19**:532.
7. Burke MF, Burke FM, Soffer DE. Review of cardiometabolic effects of prescription omega-3 fatty acids. *Curr Atheroscler Rep* 2017;**19**:60.
8. Chan DC, Pang J, Barrett PH, Sullivan DR, Mori TA, Burnett JR, van Bockxmeer FM, Watts GF. Effect of omega-3 fatty acid supplementation on arterial elasticity in patients with familial hypercholesterolaemia on statin therapy. *Nutr Metab Cardiovasc Dis* 2016;**26**:1140–1145.
9. Maki KC, Dicklin MR. Omega-3 fatty acid supplementation and cardiovascular disease risk: glass half full or time to nail the coffin shut? *Nutrients* 2018;**10**:864.
10. Bhatt DL, Steg PG, Miller M, Brinton EA, Jacobson TA, Ketchum SB, Doyle RT Jr, Juliano RA, Jiao L, Granowitz C, Tardif JC, Ballantyne CM. Cardiovascular risk reduction with icosapent ethyl for hypertriglyceridemia. *N Engl J Med* 2019;**380**:11–22.
11. Cawood AL, Ding R, Napper FL, Young RH, Williams JA, Ward MJ, Gudmundsen O, Vige R, Payne SP, Ye S, Shearman CP, Gallagher PJ, Grimble RF, Calder PC. Eicosapentaenoic acid (EPA) from highly concentrated n-3 fatty acid ethyl esters is incorporated into advanced atherosclerotic plaques and higher plaque EPA is associated with decreased plaque inflammation and increased stability. *Atherosclerosis* 2010;**212**:252–259.
12. Amano T, Matsubara T, Uetani T, Kato M, Kato B, Yoshida T, Harada K, Kumagai S, Kunimura A, Shinbo Y, Kitagawa K, Ishii H, Murohara T. Impact of omega-3 polyunsaturated fatty acids on coronary plaque instability: an integrated backscatter intravascular ultrasound study. *Atherosclerosis* 2011;**218**:110–116.
13. Shaikh SR, Edidin M. Immunosuppressive effects of polyunsaturated fatty acids on antigen presentation by human leukocyte antigen class I molecules. *J Lipid Res* 2007;**48**:127–138.
14. Kew S, Mesa MD, Tricon S, Buckley R, Minihane AM, Yaqoob P. Effects of oils rich in eicosapentaenoic and docosahexaenoic acids on immune cell composition and function in healthy humans. *Am J Clin Nutr* 2004;**79**:674–681.
15. Petursdottir DH, Hardardottir I. Dietary fish oil decreases secretion of T helper (Th) 1-type cytokines by a direct effect on murine splenic T cells but enhances secretion of a Th2-type cytokine by an effect on accessory cells. *Br J Nutr* 2008;**101**:1040–1046.
16. Iwami D, Zhang Q, Aramaki O, Nonomura K, Shirasugi N, Niimi M. Purified eicosapentaenoic acid induces prolonged survival of cardiac allografts and generates regulatory T cells. *Am J Transplant* 2009;**9**:1294–1307.
17. Shaikh SR, Jolly CA, Chapkin RS. n-3 Polyunsaturated fatty acids exert immunomodulatory effects on lymphocytes by targeting plasma membrane molecular organization. *Mol Aspects Med* 2012;**33**:46–54.
18. Hou TY, Monk JM, Fan YY, Barhoumi R, Chen YQ, Rivera GM, McMurray DN, Chapkin RS. n-3 polyunsaturated fatty acids suppress phosphatidylinositol 4, 5-

bisphosphate-dependent actin remodelling during CD4+ T-cell activation. *Biochem J* 2012;**443**:27–37.
19. Kim W, Khan NA, McMurray DN, Prior IA, Wang N, Chapkin RS. Regulatory activity of polyunsaturated fatty acids in T-cell signaling. *Prog Lipid Res* 2010;**49**:250–261.
20. Calder PC. The relationship between the fatty acid composition of immune cells and their function. *Prostaglandins Leukot Essent Fatty Acids* 2008;**79**:101–108.
21. Nicolaou A, Mauro C, Urquhart P, Marelli-Berg F. Polyunsaturated fatty acid-derived lipid mediators and T cell function. *Front Immunol* 2014;**5**:15.
22. Serhan CN, Chiang N, Van Dyke TE. Resolving inflammation: dual anti-inflammatory and pro-resolution lipid mediators. *Nat Rev Immunol* 2008;**8**:349–361.
23. O'Sullivan SE. Endocannabinoids and the cardiovascular system in health and disease. *Handb Exp Pharmacol* 2015;**231**:393–422.
24. Taltavull N, Ras R, Mariné S, Romeu M, Giralt M, Méndez L, Medina I, Ramos-Romero S, Torres JL, Nogués MR. Protective effects of fish oil on pre-diabetes: a lipidomic analysis of liver ceramides in rats. *Food Funct* 2016;**7**:3981–3988.
25. Kendall AC, Kiezel-Tsugunova M, Brownbridge LC, Harwood JL, Nicolaou A. Lipid functions in skin: differential effects of n-3 polyunsaturated fatty acids on cutaneous ceramides, in a human skin organ culture model. *Biochim Biophys Acta Biomembr* 2017;**1859**:1679–1689.
26. Chaurasia B, Summers SA. Ceramides—lipotoxic inducers of metabolic disorders. *Trends Endocrinol Metab* 2015;**26**:538–550.
27. Sreeramkumar V, Fresno M, Cuesta N. Prostaglandin E2 and T cells: friends or foes? *Immunol Cell Biol* 2012;**90**:579–586.
28. Cencioni MT, Chiurchiu V, Catanzaro G, Borsellino G, Bernardi G, Battistini L, Maccarrone M. Anandamide suppresses proliferation and cytokine release from primary human T-lymphocytes mainly via CB2 receptors. *PLoS One* 2010;**5**:e8688.
29. Arana L, Ordonez M, Ouro A, Rivera IG, Gangoiti P, Trueba M, Gomez MA. Ceramide 1-phosphate induces macrophage chemoattractant protein-1 release: involvement in ceramide 1-phosphate-stimulated cell migration. *Am J Physiol Endocrinol Metab* 2013;**304**:E1213–1226.
30. Presa N, Gomez-Larrauri A, Rivera IG, Ordonez M, Trueba M, Gomez MA. Regulation of cell migration and inflammation by ceramide 1-phosphate. *Biochim Biophys Acta* 2016;**1861**:402–409.
31. Norling LV, Headland SE, Dalli J, Arnardottir HH, Haworth O, Jones HR, Irimia D, Serhan CN, Perretti M. Proresolving and cartilage-protective actions of resolvin D1 in inflammatory arthritis. *JCI Insight* 2016;**1**:e85922.
32. Urquhart P, Parkin SM, Rogers JS, Bosley JA, Nicolaou A. The effect of conjugated linoleic acid on arachidonic acid metabolism and eicosanoid production in human saphenous vein endothelial cells. *Biochim Biophys Acta* 2002;**1580**:150–160.
33. Haas R, Smith J, Rocher-Ros V, Nadkarni S, Montero-Melendez T, D'Acquisto F, Bland EJ, Bombardieri M, Pitzalis C, Perretti M, Marelli-Berg FM, Mauro C. Lactate regulates metabolic and pro-inflammatory circuits in control of T cell migration and effector functions. *PLoS Biol* 2015;**13**:e1002202.
34. Kendall AC, Pilkington SM, Massey KA, Sassano G, Rhodes LE, Nicolaou A. Distribution of bioactive lipid mediators in human skin. *J Invest Dermatol* 2015;**135**:1510–1520.
35. Massey KA, Nicolaou A. Lipidomics of oxidized polyunsaturated fatty acids. *Free Radic Biol Med* 2013;**59**:45–55.
36. Felton SJ, Kendall AC, Almaedani AF, Urquhart P, Webb AR, Kift R, Vail A, Nicolaou A, Rhodes LE. Serum endocannabinoids and N-acyl ethanolamines and the influence of simulated solar UVR exposure in humans in vivo. *Photochem Photobiol Sci* 2017;**16**:564–574.
37. Fan YY, McMurray DN, Ly LH, Chapkin RS. Dietary (n-3) polyunsaturated fatty acids remodel mouse T-cell lipid rafts. *J Nutr* 2003;**133**:1913–1920.
38. Kendall AC, Koszyczarek MM, Jones EA, Hart PJ, Towers M, Griffiths CEM, Morris M, Nicolaou A. Lipidomics for translational skin research: a primer for the uninitiated. *Exp Dermatol* 2018;**27**:721–728.
39. Pappas A, Kendall AC, Brownbridge LC, Batchvarova N, Nicolaou A. Seasonal changes in epidermal ceramides are linked to impaired barrier function in acne patients. *Exp Dermatol* 2018;**27**:833–836.
40. Ratajczak MZ, Suszynska M, Borkowska S, Ratajczak J, Schneider G. The role of sphingosine-1 phosphate and ceramide-1 phosphate in trafficking of normal stem cells and cancer cells. *Expert Opin Ther Targets* 2014;**18**:95–107.
41. Joseph J, Niggemann B, Zaenker KS, Entschladen F. Anandamide is an endogenous inhibitor for the migration of tumor cells and T lymphocytes. *Cancer Immunol Immunother* 2004;**53**:723–728.
42. Kalinski P. Regulation of immune responses by prostaglandin E2. *J Immunol* 2012;**188**:21–28.
43. Pilkington SM, Murphy SA, Kudva S, Nicolaou A, Rhodes LE. COX inhibition reduces vasodilator PGE2 but is shown to increase levels of chemoattractant 12-HETE in vivo in human sunburn. *Exp Dermatol* 2015;**24**:790–791.
44. Cantrell DA. GTPases and T cell activation. *Immunol Rev* 2003;**192**:122–130.
45. Rougerie P, Delon J. Rho GTPases: masters of T lymphocyte migration and activation. *Immunol Lett* 2012;**142**:1–13.
46. Amano M, Ito M, Kimura K, Fukata Y, Chihara K, Nakano T, Matsuura Y, Kaibuchi K. Phosphorylation and activation of myosin by Rho-associated kinase (Rho-kinase). *J Biol Chem* 1996;**271**:20246–20249.
47. Manser E, Leung T, Salihuddin H, Zhao ZS, Lim L. A brain serine/threonine protein kinase activated by Cdc42 and Rac1. *Nature* 1994;**367**:40–46.
48. Bokoch GM. Biology of the p21-activated kinases. *Annu Rev Biochem* 2003;**72**:743–781.
49. Ratajczak MZ, Adamiak M. Membrane lipid rafts, master regulators of hematopoietic stem cell retention in bone marrow and their trafficking. *Leukemia* 2015;**29**:1452–1457.
50. Head BP, Patel HH, Insel PA. Interaction of membrane/lipid rafts with the cytoskeleton: impact on signaling and function: membrane/lipid rafts, mediators of cytoskeletal arrangement and cell signaling. *Biochim Biophys Acta* 2014;**1838**:532–545.
51. Lin BJ, Tsao SH, Chen A, Hu SK, Chao L, Chao PG. Lipid rafts sense and direct electric field-induced migration. *Proc Natl Acad Sci USA* 2017;**114**:8568–8573.
52. Mammoto A, Huang S, Ingber DE. Filamin links cell shape and cytoskeletal structure to Rho regulation by controlling accumulation of p190RhoGAP in lipid rafts. *J Cell Sci* 2007;**120**:456–467.
53. Wang R, Bi J, Ampah KK, Ba X, Liu W, Zeng X. Lipid rafts control human melanoma cell migration by regulating focal adhesion disassembly. *Biochim Biophys Acta* 2013;**1833**:3195–3205.
54. Dong YQ, Zhang XZ, Sun LL, Zhang SY, Liu B, Liu HY, Wang X, Jiang CT. Omega-3 PUFA ameliorates hyperhomocysteinemia-induced hepatic steatosis in mice by inhibiting hepatic ceramide synthesis. *Acta Pharmacol Sin* 2017;**38**:1601–1610.
55. Shang T, Liu L, Zhou J, Zhang M, Hu Q, Fang M, Wu Y, Yao P, Gong Z. Protective effects of various ratios of DHA/EPA supplementation on high-fat diet-induced liver damage in mice. *Lipids Health Dis* 2017;**16**:65.
56. Laguna-Fernandez A, Checa A, Carracedo M, Artiach G, Petri MH, Baumgartner R, Forteza MJ, Jiang X, Andonova T, Walker ME, Dalli J, Arnardottir H, Gisterå A, Thul S, Wheelock CE, Paulsson-Berne G, Ketelhuth DFJ, Hansson GK, Bäck M. ERV1/ChemR23 signaling protects against atherosclerosis by modifying oxidized low-density lipoprotein uptake and phagocytosis in macrophages. *Circulation* 2018;**138**:1693–1705.
57. Chiurchiu V, Leuti A, Dalli J, Jacobsson A, Battistini L, Maccarrone M, Serhan CN. Proresolving lipid mediators resolvin D1, resolvin D2, and maresin 1 are critical in modulating T cell responses. *Sci Transl Med* 2016;**8**:353ra111.
58. Wassall SR, Leng X, Canner SW, Pennington ER, Kinnun JJ, Cavazos AT, Dadoo S, Johnson D, Heberle FA, Katsaras J, Shaikh SR. Docosahexaenoic acid regulates the formation of lipid rafts: a unified view from experiment and simulation. *Biochim Biophys Acta Biomembr* 2018;**1860**:1985–1993.
59. Kosaraju R, Guesdon W, Crouch MJ, Teague HL, Sullivan EM, Karlsson EA, Schultz-Cherry S, Gowdy K, Bridges LC, Reese LR, Neufer PD, Armstrong M, Reisdorph N, Milner JJ, Beck M, Shaikh SR. B Cell activity is impaired in human and mouse obesity and is responsive to an essential fatty acid upon murine influenza infection. *J Immunol* 2017;**198**:4738–4752.
60. Cai W, Liu S, Hu M, Sun X, Qiu W, Zheng S, Hu X, Lu Z. Post-stroke DHA treatment protects against acute ischemic brain injury by skewing macrophage polarity toward the M2 phenotype. *Transl Stroke Res* 2018;**9**:669–680.
61. Kong W, Yen JH, Ganea D. Docosahexaenoic acid prevents dendritic cell maturation, inhibits antigen-specific Th1/Th17 differentiation and suppresses experimental autoimmune encephalomyelitis. *Brain Behav Immun* 2011;**25**:872–882.

Translational perspective

The n-3PUFA EPA and DHA, found in fish oils, have been explored as means of preventing cardiovascular disease and improving cardiometabolic risk factors. Although the efficiency of n-3PUFA is debated, recent clinical studies have shown that EPA supplementation can reduce the risk of ischemic events and increase the stability of the atherosclerotic plaque, with EPA plaque levels inversely related to their T cell content. While the immunomodulatory properties of n-3PUFA are appreciated, the underpinning molecular mechanisms are not fully understood. Our data add to our understanding of the immunomodulatory properties of n-3PUFA and their beneficial effects.